

Odorant Representations Are Modulated by Intra- but Not Interglomerular Presynaptic Inhibition of Olfactory Sensory Neurons

John P. McGann,^{1,*} Nicolás Pérez,¹ Melanie A. Gainey,¹ Christina Muratore,¹ Adam S. Elias,¹ and Matt Wachowiak¹

¹ Department of Biology
Boston University
5 Cummington Street
Boston, Massachusetts 02215

Summary

Input to the central nervous system from olfactory sensory neurons (OSNs) is modulated presynaptically. We investigated the functional organization of this inhibition and its role in odor coding by imaging neurotransmitter release from OSNs in slices and in vivo in mice expressing synaptophluorin, an optical indicator of vesicle exocytosis. Release from OSNs was strongly suppressed by heterosynaptic, intraglomerular inhibition. In contrast, inhibitory connections between glomeruli mediated only weak lateral inhibition of OSN inputs in slices and did not do so in response to odorant stimulation in vivo. Blocking presynaptic inhibition in vivo increased the amplitude of odorant-evoked input to glomeruli but had little effect on spatial patterns of glomerular input. Thus, intraglomerular inhibition limits the strength of olfactory input to the CNS, whereas interglomerular inhibition plays little or no role. This organization allows for control of input sensitivity while maintaining the spatial maps of glomerular activity thought to encode odorant identity.

Introduction

The first synapse in the olfactory pathway is critical in generating central representations of odors. Here, several thousand olfactory sensory neurons (OSNs), all expressing the same olfactory receptor protein, converge onto many fewer postsynaptic targets within an anatomically discrete neuropile called a glomerulus (Mombaerts et al., 1996; Treloar et al., 2002). Each glomerulus represents a single olfactory receptor type and serves as a functional unit for processing and coding olfactory information (Shepherd et al., 2004; Bozza et al., 2002; Wachowiak et al., 2004). The most abundant synaptic connection within each glomerulus is the excitatory, glutamatergic contact between OSNs and second-order neurons (Kasowski et al., 1999). Signal transmission at this synapse can be modulated presynaptically via several pathways, including depression intrinsic to the presynaptic terminal (Murphy et al., 2004) and GABA- and dopaminergic synaptic inhibition (Aroniadou-Anderjaska et al., 2000; Ennis et al., 2001; Wachowiak and Cohen, 1999; Wachowiak et al., 2005). Despite its importance in controlling information flow in the olfactory bulb, the role of presynaptic inhibition in odor coding remains

unexplored. A number of functions have been hypothesized, including modulating sensitivity, attenuating postsynaptic responses during repeated sniffing, and sharpening odorant response patterns via lateral inhibition (Aroniadou-Anderjaska et al., 2000; Aungst et al., 2003; Duchamp-Viret et al., 2000; Ennis et al., 2001). Ultimately, the role of presynaptic inhibition in odor coding depends on the functional organization of the underlying circuitry and the nature of its activation by odorants.

Understanding this organization is difficult because of the complex synaptic connections within and between glomeruli. For example, feedback inhibition within a glomerulus can occur when periglomerular interneurons (PG cells) are excited by OSNs and in turn presynaptically inhibit further OSN input (Murphy et al., 2005; Wachowiak et al., 2005). But PG cells are also activated by other sources, including mitral and tufted cell dendrites in the same glomerulus (Murphy et al., 2005), and short-axon cells originating in neighboring glomeruli (Aungst et al., 2003). The short-axon cell connections mediate inhibition between glomeruli by activating inhibitory, PG cell input to mitral cells, which may serve to sharpen odorant representations (Aungst et al., 2003). However, whether this circuit also presynaptically inhibits OSN input is unclear. Testing these and other hypotheses has been limited in part because of the difficulty in measuring presynaptic inhibition directly: OSN terminals are inaccessible to electrodes and the complex glomerular circuitry makes it difficult to infer presynaptic mechanisms based on electrophysiological recordings from postsynaptic cells.

Here, we address this problem by imaging transmitter release directly from OSN axon terminals using synaptophluorin (spH), a genetically-encoded indicator of vesicle exocytosis (Miesenböck et al., 1998; Ng et al., 2002; Bozza et al., 2004). We first used in vitro slice preparations to characterize three pathways by which transmitter release is modulated by prior olfactory input: intrinsic paired-pulse depression of release; intraglomerular, feedback inhibition of release; and lateral, interglomerular inhibition. We then asked how the latter two pathways shape odor representations in vivo. We found that intraglomerular feedback inhibition strongly modulates the magnitude of OSN input to the glomerulus but that interglomerular presynaptic inhibition plays little or no role in shaping relative patterns of glomerular input. We conclude that presynaptic inhibition regulates the strength of olfactory input to the CNS while maintaining spatial representations of odor information.

Results

Imaging Transmitter Release from OSNs

To monitor the presynaptic modulation of transmitter release from OSN axons, we imaged evoked fluorescence signals in mice (OMP-spH) in which spH expression is driven from the olfactory marker protein (OMP) locus. OMP-spH mice show strong and selective expression of spH in virtually all OSNs (Bozza et al., 2004). We earlier

*Correspondence: mcgann@bu.edu

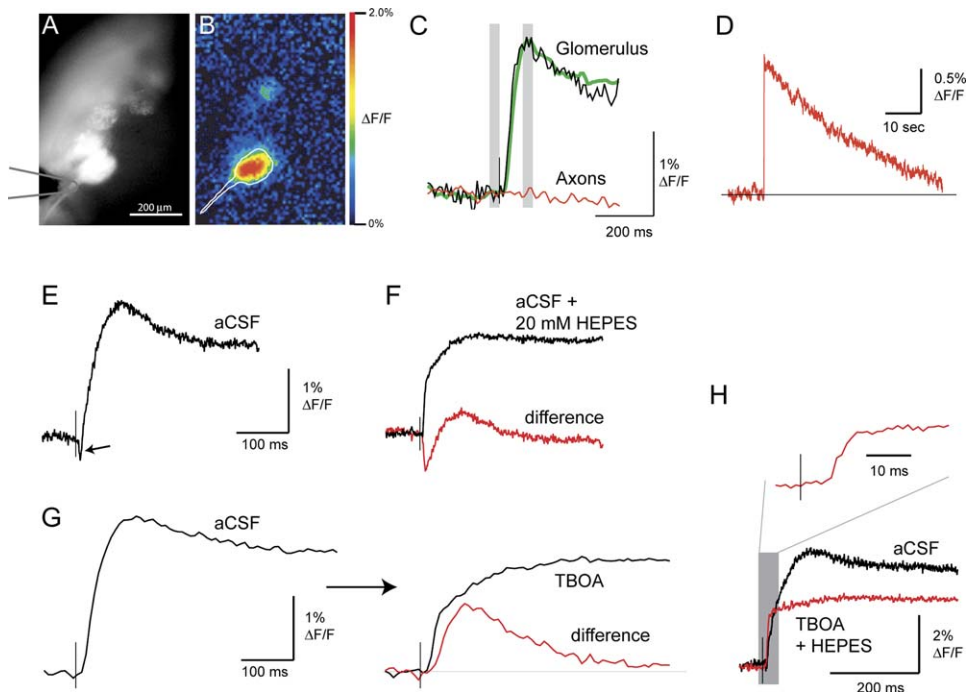


Figure 1. SynaptopHluorin Signals Imaged from OSN Terminals In Vitro

(A–C) Resting fluorescence of an olfactory bulb slice from an OMP-spH mouse. Individual glomeruli and a bundle of OSN axons are visible. The position of the stimulating electrode used to evoke the signal in (B) and (C) is indicated in gray. (B) Pseudocolor map of the fluorescence increase evoked by a single ON shock. The frames used for creating the response map are indicated in (C). The signal is strongest in the glomerulus nearest the stimulating electrode; a small response is also visible in a second glomerulus that is slightly out of focus. (C) Time course of the ON-evoked spH signal measured from the glomerulus in (A). Black trace shows the unfiltered spH fluorescence from a single trial, imaged at 125 Hz. Green trace shows the signal averaged across eight trials and low-pass filtered at 20 Hz. Red trace shows the signal from pixels overlying the axon, also averaged and filtered. Gray bars indicate the frames used to produce the response map in (B). Thin vertical line indicates time of ON shock.

(D) Long imaging record, obtained from a different preparation, demonstrating the slow decay of the ON-evoked spH signal. Trace is average of four trials, imaged at 40 Hz.

(E) Trace of ON-evoked spH signal imaged from a different glomerulus at 1 kHz frame rate reveals complex signal kinetics. The response begins with a small and rapid decrease in fluorescence (arrow), followed by a slower rise and an initial decay with time constant of ~ 90 ms. Trace is average of four trials and is unfiltered.

(F) Black trace shows the spH signal measured from the same glomerulus as in (E) after switching to aCSF containing 20 mM HEPES. The initial fluorescence decrease is eliminated and the rise time is faster. The difference between the traces in (E) and (F) (red trace) reveals the buffering-dependent component of the evoked signal, which consists of a rapid acidification of the synaptic cleft followed by a slower alkalization.

(G) The slower alkalization is mediated by glutamate transporters. Left trace shows ON-evoked spH signal imaged from a different glomerulus in control aCSF (four-trial average, imaged at 125 Hz). Right trace shows response in 50 μ M TBOA (black) and difference between control and TBOA traces (red). The alkalization is likely due to cotransport of protons by the glutamate transporter.

(H) ON-evoked spH signals show a rapid and simple fluorescence increase in 20 mM HEPES-buffered aCSF and TBOA (red) without the complex kinetics seen in control aCSF (black). Traces are four-trial averages imaged at 2 kHz and unfiltered. Inset (above) shows the evoked signal in HEPES and TBOA on an expanded time scale. The rise time of the spH signal is <10 ms.

used OMP-spH mice to image odor representations in vivo (Bozza et al., 2004) and more recently demonstrated their ability to report olfactory nerve (ON) shock evoked transmitter release in olfactory bulb slice preparations (Wachowiak et al., 2005). Figure 1 illustrates basic features of the ON-evoked spH signal. A single ON shock evokes a fluorescence increase in one or more glomeruli (Figures 1A–1C). No fluorescence change is observed in axons distal to the glomerulus or in subglomerular layers (Figures 1B and 1C). Application of 1 μ M tetrodotoxin to block axonal conduction completely eliminated evoked spH signals (reduced to $0.0\% \pm 1.0\%$ of control; $n = 9$ glomeruli from two slices). SpH signal amplitude is graded with stimulus intensity, likely reflecting increases in the number of activated OSN fibers (not shown, but see Figure 5 from Wachowiak

et al., [2005]). In slices, spH signals typically have a maximal amplitude of 1%–2% $\Delta F/F$.

In cultured neurons imaged at low temporal resolution, presynaptic stimulus trains elicit a rapid fluorescence increase followed by a slow decay lasting many seconds to minutes (Sankaranarayanan and Ryan 2000; Gandhi and Stevens 2003; Li et al., 2005). ON-evoked spH signals in olfactory bulb slices showed a similarly slow decay, with an $83\% \pm 3\%$ return to baseline fluorescence 50 s after a single ON shock ($n = 8$ glomeruli, three slices) (Figure 1D). High frame-rate imaging revealed that the onset kinetics of the spH signal were more complex than reported previously. The ON-evoked fluorescence increase was unexpectedly slow, with a half-maximal rise time of 32.2 ± 2.6 msec (mean \pm SEM; $n = 16$ glomeruli; four slices) and time to peak of

94.7 ± 5.4 msec. In addition, the fluorescence increase was preceded by a brief decrease in fluorescence (Figure 1E). This initial response was followed by a somewhat rapid decay in fluorescence (90 ms decay time constant; n = 11 glomeruli from six slices; Figure 1D), after which the fluorescence decayed slowly as described above.

These complex kinetics may reflect pH changes in the synaptic cleft because of the synchronous release and removal of transmitter (and associated protons) from many OSN terminals. To test this idea, we first tested the effects of a modified artificial cerebrospinal fluid (aCSF) containing 20 mM HEPES to increase its pH-buffering capacity (see [Experimental Procedures](#)). In this HEPES-aCSF, the initial fluorescence decrease was eliminated, and the kinetics of the fluorescence increase were accelerated (Figure 1F). Subtracting the response traces obtained before and after switching to HEPES-aCSF revealed a transient fluorescence decrease representing an acidification of the synaptic cleft (Figure 1F). The transient had a latency of 3.3 ± 0.3 ms (n = 15 glomeruli, three slices), a time to peak (maximal fluorescence decrease) of 5.3 ± 0.3 ms (n = 15) and a decay time constant of 32 ± 4 ms (n = 15). Because protons are cotransported during glutamate reuptake, reuptake of glutamate from the synaptic cleft may also alter local pH (Zerangue and Kavanaugh, 1996). To test this, we blocked glutamate reuptake (in normal aCSF) with the nonspecific excitatory amino acid transporter blocker DL-threo-*b*-benzyloxycarboxylate (TBOA). TBOA slowed the initial fluorescence increase and eliminated the rapid decay phase of the ON-evoked spH signal (Figure 1G). Subtracting traces obtained before and after TBOA addition revealed a transient alkalization after ON shock (Figure 1G). The reuptake transient had a latency of 9.6 ± 0.7 msec (n = 4 glomeruli sampled at 2 kHz frame rate), reached peak amplitude 96 ± 6 ms after ON shock (n = 9 glomeruli; two slices), and decayed with a time constant of 109 ± 25 ms (n = 5 glomeruli; two slices). Adding HEPES and TBOA simultaneously nearly eliminated all complex kinetics, resulting in a simple fluorescence increase with short but measurable latency (3.4 ± 0.3 ms) and rapid rise time (time-to-half max, 4.7 ± 0.4 ms; n = 5 glomeruli measured at 2 kHz frame rate), consistent with the kinetics of ON-evoked transmitter release from OSN terminals (Keller et al., 1998; Wachowiak et al., 2005). Thus, pH changes in the synaptic cleft because of transmitter release and reuptake can contribute significantly to the initial kinetics of the ON-evoked spH signal.

Despite the contributions of these additional sources, we have reported that peak spH signal amplitude is linearly related to the amplitude of monosynaptic EPSCs recorded electrophysiologically and supralinearly related to $[Ca^{2+}]_{ext}$ and that the rise time of the spH signal is independent of its amplitude (Wachowiak et al., 2005). These results suggest that both the direct and indirect release-related components of the spH signal scale approximately linearly with the amount of transmitter released from OSN terminals. Thus, to simplify the design and analysis of subsequent experiments, we used peak spH amplitude (typically measured at ~100 ms post ON shock) to measure the presynaptic modulation of transmitter release from OSNs.

Suppression of Transmitter Release from OSNs

Transmitter release from OSNs is regulated by multiple mechanisms, including activity-dependent depression intrinsic to the presynaptic terminal (Murphy et al., 2004) and synaptically mediated presynaptic inhibition (Aroniadou-Anderjaska et al., 2000; Ennis et al., 2001; Wachowiak et al., 2005). As expected, ON-evoked spH signals showed strong paired-pulse suppression. The time course of this suppression was biphasic, with a slow onset and a slower recovery (Figures 2A and 2B). The suppression ratio (SR, test response/control response) at an interstimulus interval (ISI) of 10 ms was 0.60 ± 0.05 (n = 9 glomeruli, five slices) but decreased to a minimum of 0.09 ± 0.02 (n = 23 glomeruli, nine slices) at 200 msec ISIs and recovered slowly over the next 10 s (Figures 2A and 2B). This time course is much slower than the recovery cycle of the olfactory nerve, which has been reported to have an absolute refractory period of ~3 ms and relative refractory period that ends within 15–30 ms (Getchell and Shepherd, 1975). To minimize the confound of the initial response kinetics in this analysis, we made all test response measurements at ISIs < 300 ms after subtracting traces evoked by the conditioning stimulus alone (see [Experimental Procedures](#) for details). Further, in a subset of glomeruli analyzed, the initial kinetics of the in vitro spH signal did not appear to affect the measurement of presynaptic inhibition, as the suppression ratio computed from the peaks of the spH responses was not different than that by measuring response amplitude at 280 msec poststimulus, after the pH- and reuptake-dependent components of the response had decayed, and found identical paired-pulse suppression (400 ms ISI; PPR measured at peak: 0.14 ± 0.02; PPR measured 280 ms after peak: 0.11 ± 0.02; paired t test; p = 0.17).

To assess what portion of paired-pulse suppression is synaptically mediated, we blocked evoked postsynaptic activity with NBQX and AP-5 (20 μM and 100 μM, respectively). NBQX/AP-5 had no effect on the conditioning response (amplitude: 96% ± 3% of control; n = 19; one-group t test, p = 0.471) but reduced paired-pulse suppression (Figures 2C and 2D). Application of AP-5 alone (to preferentially block dendritic glutamate release) (see Isaacson and Strowbridge, 1998; Chen et al., 2000) produced only a small reduction in paired-pulse suppression (15 glomeruli in four slices) (see Figure 2E). Selectively blocking GABA_B-mediated presynaptic inhibition with CGP55845 (50 μM) had a similar effect to glutamate receptor blockade (Figures 2C and 2D). CGP55845 did not change the amplitude of the conditioning response, nor did it alter the time constant of the initial decay phase of the response (predrug: 89.9 msec; postdrug = 78.7 msec; averaged waveform across five glomeruli from two slices) or the later, slowly-decaying phase (summed difference between control and CGP55845 responses for all frames 3 s poststimulus, 0.23% ± 0.03% ΔF/F versus 0.12% ± .004% ΔF/F for 3 s prestimulus; paired t test, p = 0.08; n = 9 glomeruli, three slices) (Figure 2D). As in control aCSF, the suppression ratio observed in CGP55845 was the same whether it was measured at the peak of the spH response or 280 msec after the peak (paired t test; p = 0.11). With both CGP and NBQX/AP-5, suppression

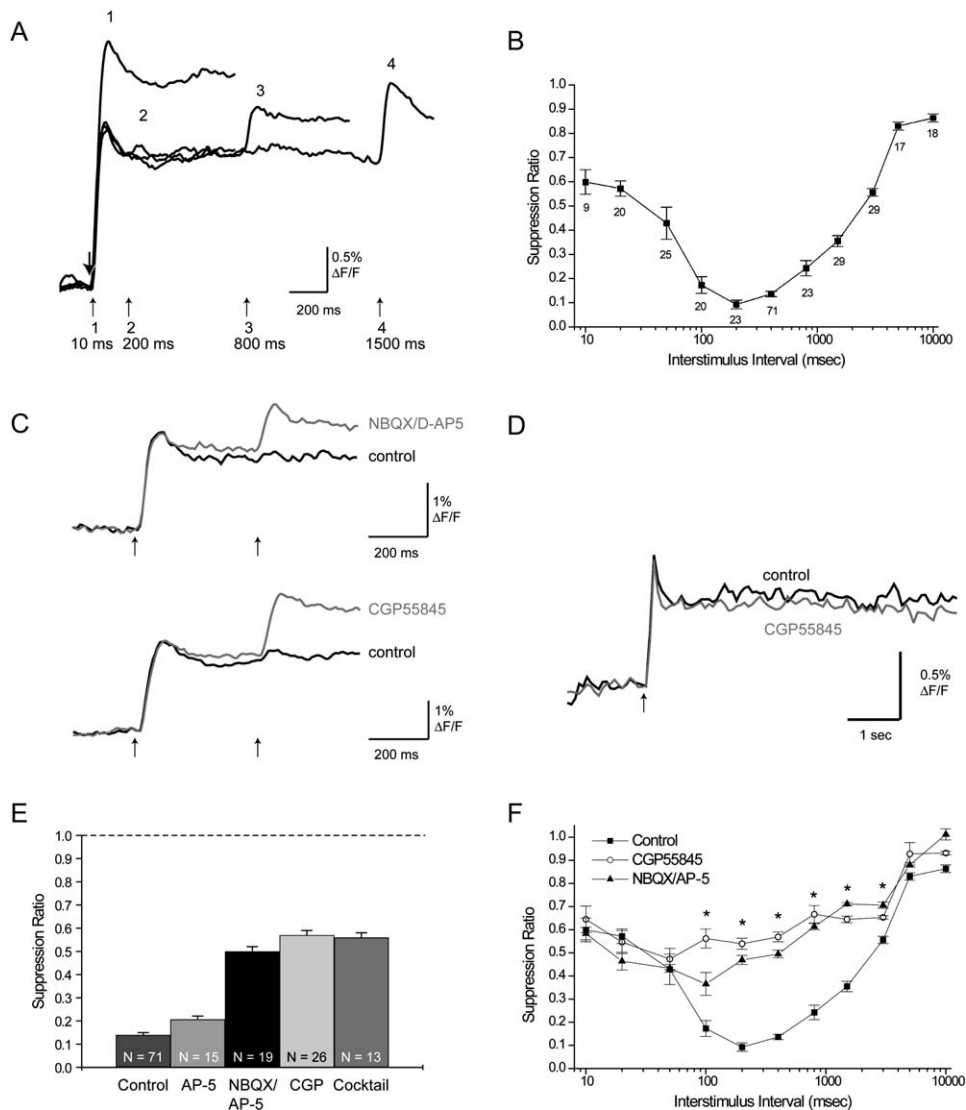


Figure 2. Paired-Pulse Suppression of Transmitter Release Imaged with spH

(A) Overlaid traces showing spH signals evoked by paired-pulse stimulation at four different ISIs. Large downward arrow indicates the time of the conditioning pulse. Small numbered arrows correspond to each trace and indicate time of test pulse and ISI. The test response at 10 ms ISI (1) is large but is almost completely suppressed at 200 msec ISI (2). There is gradual recovery of test response amplitude over 1.5 s.

(B) Plot of suppression ratio (SR) versus ISI, with time plotted logarithmically. Paired-pulse suppression is apparent immediately but reaches peak amplitude only after 100–200 msec and recovers over the next 10 s. Symbols and error bars in this and all other plots indicate mean ± SEM. Numbers below each point indicate number of glomeruli tested at each interval.

(C) Blockade of ionotropic glutamate receptors with NBQX/AP-5 (upper traces) reduces paired-pulse suppression without affecting the response to the conditioning pulse. Blockade of GABA_B receptors with CGP55845 produces a comparable effect (lower traces). Traces show responses to paired ON shock at 400 ms ISI.

(D) CGP55845 has no effect on either the amplitude or long-term kinetics of the spH signal evoked by a single ON shock. Traces show the evoked signal (seven-trial average; 40 Hz frame rate) for 6 s after ON shock before and after CGP55845 addition.

(E) Summary data of effect of 100 μM AP-5, 20 μM NBQX/100 μM AP-5, 50 μM CGP55845, or a cocktail of all three plus 100 μM sulpiride, a D₂ dopamine receptor antagonist, on paired-pulse suppression (400 ms ISI), compared to control values. Each treatment relieved suppression, but significant suppression remained in all cases.

(F) Plot of SR versus ISI after glutamate receptor blockade (NBQX/AP-5 plot) or GABA_B receptor blockade (CGP55845 plot), compared with control values (control plot, same data as shown in [B]). Asterisks indicate ISIs showing a significant difference between synaptically and nonsynaptically mediated suppression ($p < 0.05$ for both drugs). Note that there is no difference at ISIs <100 msec.

was unchanged by drug application at ISIs ≤ 50 ms (Figure 2F; Fisher's PLSD, all $p > 0.10$) but was significantly reduced by both drugs at ISIs from 100 ms to 3 s (Figure 2F; Fisher's PLSD, $p < 0.05$). Blocking all known sources of presynaptic inhibition with a cocktail of AP-5 (100 μM), CNQX (20 μM), CGP55845 (50 μM)

and the D₂ antagonist sulpiride (100 μM) increased the SR from 0.11 ± 0.01 to 0.56 ± 0.02 (400 ms ISI; $n = 13$), a value similar to the effect of NBQX/AP-5 or CGP55845 alone (Figure 2E).

Thus, synaptically mediated inhibition of transmitter release from OSNs has a slow onset and an even

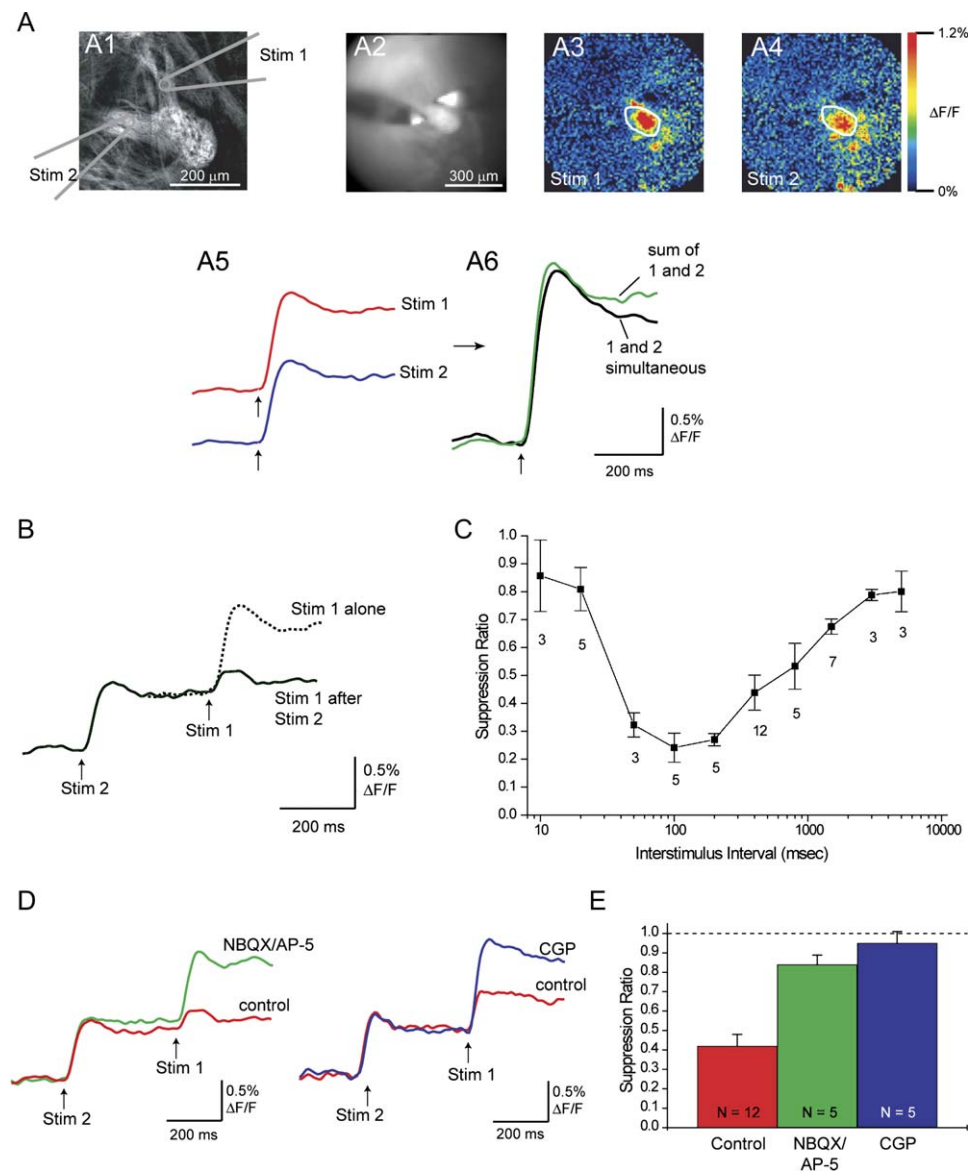


Figure 3. Heterosynaptic, Intraglomerular Presynaptic Inhibition of Transmitter Release from OSNs

(A) Experimental configuration for heterosynaptic inhibition experiments. (A1) Confocal image of a glomerulus innervated by two separate bundles of OSN axons. The positions of the two stimulating electrodes (see A2) are drawn in gray. (A2) Resting fluorescence of the same glomerulus and stimulating electrodes as imaged during the experiment. (A3–A4) Pseudocolor maps of the fluorescence increase evoked by a single ON shock from electrodes 1 (A3) and 2 (A4). (A5) Traces showing the pH signals from the glomerulus evoked by each electrode. (A6) Traces showing the actual signal evoked by stimulating with both electrodes simultaneously (black trace) and the linear sum of the signals evoked by each electrode alone (green trace). The similar amplitude of these traces demonstrates that the electrodes activate nonoverlapping populations of axons. (B) Traces from the glomerulus shown in (A) illustrating suppression of the pH signal evoked by electrode 1 after a conditioning stimulus on electrode 2 (400 msec ISI). (C) Plot of average SR across experiments versus ISI. Note the difference from Figure 2B at short ISIs. Numbers below each point indicate the number of glomeruli tested at each ISI. Error bars indicate SEM. (D) Blockade of ionotropic glutamate receptors with NBQX/AP-5 (left traces) reduces paired-pulse suppression. Blockade of GABA_B receptors with CGP55845 produces a comparable effect (right traces). Traces show responses to paired ON shock (400 ms ISI). (E) Summary data showing the effects of NBQX/AP-5 or CGP55845 (400 msec ISI). Dotted line indicates an SR of 1 (no suppression).

slower decay, consistent with its being mediated by metabotropic GABA_B and D₂ dopamine receptors (Aroniadou-Anderjaska et al., 2000; Ennis et al., 2001), and has its largest impact on release at ISIs between 100–1000 msec. We next designed a series of experiments to understand the functional organization of presynaptic inhibition within the glomerular layer of the olfactory bulb and its potential role in odor coding.

Intraglomerular Feedback Inhibition of Transmitter Release Is Strong In Vitro

We first asked whether inhibition within a glomerulus modulates transmitter release from OSNs. To eliminate the contribution of intrinsic synaptic depression, we used a two-electrode stimulation paradigm to selectively activate different OSNs innervating the same glomerulus. Figure 3A1 shows an example of this configuration;

typically, it was possible to visually place each electrode on a separate fiber bundle innervating the glomerulus of interest. In most cases, each electrode evoked spH signals in the same area within the glomerulus (Figures 3A2–3A4), indicating that the axon terminals from each bundle were intermingled. We ensured the selective activation of different OSN axons by each electrode by requiring that simultaneous stimulation with both electrodes evoke a fluorescence increase $\geq 80\%$ of the sum of the responses to each electrode individually (Figure 3A5 and 3A6). In some experiments ($n = 6$), we further confirmed that the stimulated bundles innervated the same glomerulus by post-hoc three-dimensional reconstruction on a confocal microscope.

Successive shocks delivered to the two ON electrodes ($n = 12$ glomeruli) revealed strong heterosynaptic, feedback inhibition of transmitter release from OSNs (Figure 3B). The mean SR evoked by a single conditioning pulse (tested at 400 ms ISI) was 0.42 ± 0.06 ($n = 12$ glomeruli). Heterosynaptic inhibition had a slow onset, reaching peak magnitude 100 msec after the conditioning pulse and decaying slowly over the next 1–3 s (Figure 3C). This suppression was nearly eliminated by NBQX/AP-5 (SR = 0.84 ± 0.05 ; $n = 5$) and completely eliminated by CGP55845 (SR = 0.95 ± 0.06 ; $n = 5$) (Figures 3D and 3E). The small residual inhibition in the presence of NBQX/AP-5 may reflect direct activation of GABAergic PG cells by the stimulating electrode. In two experiments, we measured intraglomerular inhibition at 36°C in addition to our normal measurement at 30°C. In both cases the suppression was weaker at the higher temperature but still strong (SR, 400 ms ISI, at 30°C = 0.30 ± 0.06 ; SR at 36°C = 0.52 ± 0.07).

These experiments show that feedback inhibition from GABAergic local interneurons can strongly suppress OSN input to a glomerulus and further show that activation of one set of glomerular inputs can suppress release from another set of inputs to the same glomerulus.

Lateral Presynaptic Inhibition between Glomeruli Is Weak In Vitro

A subclass of juxtglomerular interneurons—the short axon cells—mediate lateral inhibitory interactions between nearby glomeruli by exciting periglomerular interneurons, which in turn inhibit mitral cells (Aungst et al., 2003). Periglomerular cell activation can also cause presynaptic inhibition of OSN input (Murphy et al., 2005). We asked whether lateral, interglomerular inhibition acts presynaptically, with OSN input to one glomerulus inhibiting afferent input to neighboring glomeruli. We again used a dual-electrode stimulus paradigm, but this time, each electrode selectively activated different glomeruli (Figures 4A and 4B). In these experiments, the interglomerular synaptic network was preserved with “surface slices” cut tangentially from the dorsal or lateral bulb (Aungst et al., 2003). Similar results were obtained in a small number of transverse slices (data not shown).

In 18 experiments (slices from 13 mice), we imaged from 45 glomeruli that exhibited a response to only one of the two electrodes (see Figures 4A and 4B). For each glomerulus, we compared its evoked response alone and after evoking input to its neighbors with the other electrode (Figure 4B). Using this paradigm, we found

that activation of neighboring glomeruli could, in some cases, suppress the ON-evoked spH signal in the test glomerulus, demonstrating that lateral connections in the glomerular layer can in fact mediate presynaptic inhibition between glomeruli.

Compared to the intraglomerular inhibition experiments, lateral inhibition of OSN input was weak. For all glomeruli less than 400 μm from an activated neighbor, the mean SR was 0.88 ± 0.03 (400 ms ISI; $n = 33$) (Figure 4C), which was statistically significant (one-group *t* test, $p < 0.001$) but much weaker than the SR for the heterosynaptic intraglomerular inhibition experiments (SR = 0.42). The lowest SR ever observed was 0.46, compared with a minimum SR of 0.07 for the intraglomerular experiments. Lateral inhibition was also limited by distance: glomeruli more than 400 μm from the nearest activated neighbor showed no significant suppression (mean SR = 1.02 ± 0.03 ; $n = 8$; unpaired *t* test) (Figure 4C).

We further characterized interglomerular inhibition in a subset of glomeruli showing an SR of 0.9 or less. Although lateral inhibition showed the same delayed onset as did intraglomerular feedback inhibition, its magnitude was smaller at all ISIs, and the duration of detectable suppression was shorter (Figure 4D). As expected, suppression by neighboring glomeruli was eliminated by NBQX/AP-5 (SR_{pre} = 0.70 ± 0.04 ; SR_{drug} = 0.97 ± 0.02 ; $n = 5$; $p = 0.005$) and by CGP55845 (SR_{pre} = 0.74 ± 0.02 ; SR_{drug} = 0.98 ± 0.01 ; $n = 5$; $p < 0.001$) (Figure 4E). Finally, as for intraglomerular inhibition, increasing the bath temperature from 30°C to 36°C caused a small but significant reduction in lateral inhibition (SR, 30°C = 0.71 ± 0.08 ; SR, 36°C = 0.80 ± 0.06 ; paired *t* test; $n = 4$ glomeruli from three slices; $p < 0.026$). Thus, OSN inputs to a glomerulus can suppress input to its neighbors, but this inhibition is much weaker than feedback inhibition within the same glomerulus.

Lateral Presynaptic Inhibition Does Not Alter Odorant Representations In Vivo

Having characterized these two modes of presynaptic inhibition in slices, we next asked how each mode affects odorant representations in vivo. First, to address whether lateral inhibition modulates odorant-evoked input to glomeruli, we designed an in vivo analog to the slice experiments with different odorants to selectively evoke input to neighboring glomeruli. We reasoned that if interglomerular inhibition modulates OSN input in vivo, then the odorant-evoked spH signal in a test glomerulus would be suppressed when its neighbor was coactivated by a different odorant.

The experimental design is illustrated in Figure 5B. In this example, butyl acetate evokes strong input to a single glomerulus (the “test glomerulus”) in the anterior-medial domain of the dorsal bulb and weaker input to additional glomeruli (Figure 5B, left). A different odorant, methyl valerate, evokes strong input to many glomeruli surrounding the test glomerulus but evokes little input to the test glomerulus itself (Figure 5B, middle). We then asked whether coactivation of the surrounding glomeruli by methyl valerate suppressed the response of the test glomerulus to butyl acetate by presenting the two odorants as a binary mixture (Figure 5B, right). As shown in Figure 5C, the test glomerulus’ response to the mixture was identical in both amplitude and time

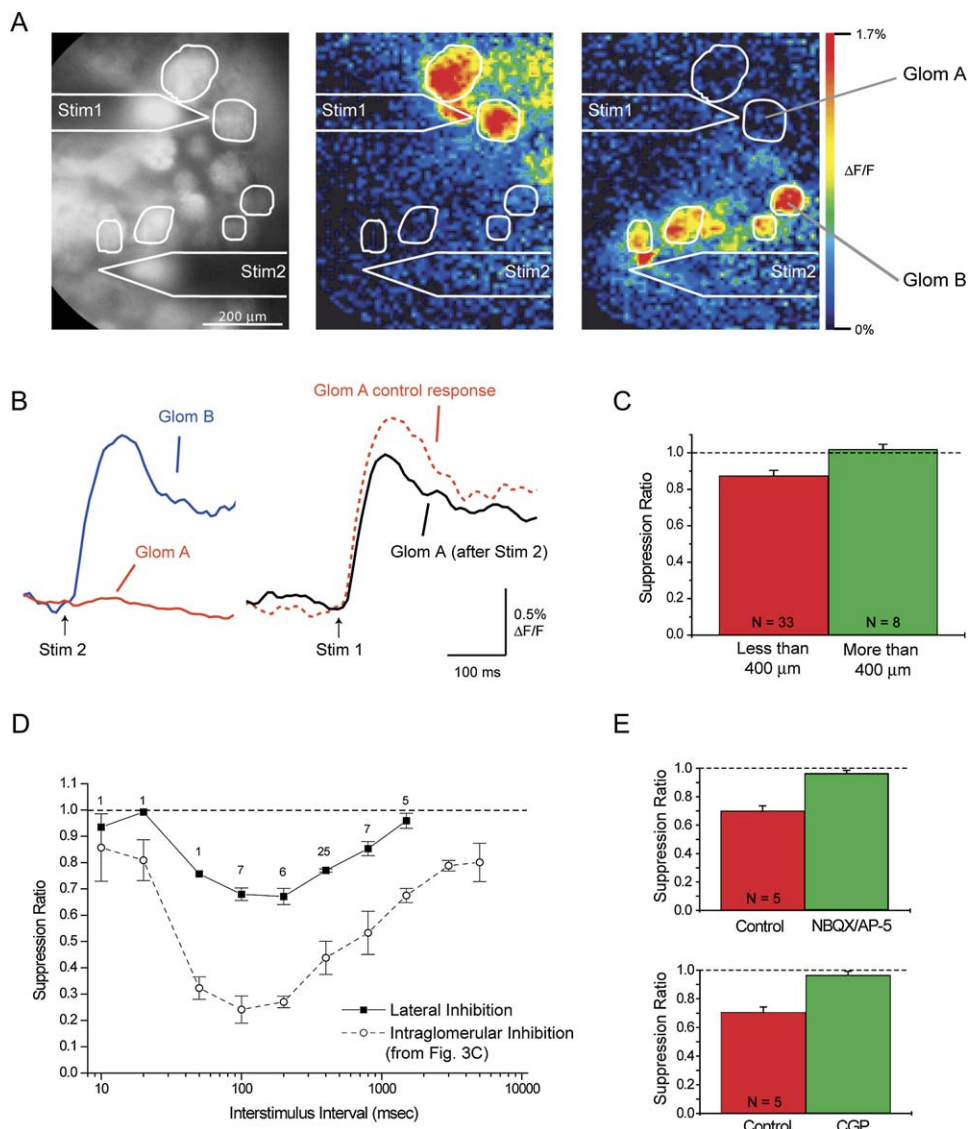


Figure 4. Interglomerular Presynaptic Inhibition of Transmitter Release In Vitro

(A) Experimental configuration of interglomerular inhibition experiments. (Left) Resting pH fluorescence of glomeruli in an olfactory bulb surface slice. Certain responsive glomeruli are outlined, as are the two stimulating electrodes. Pseudocolor maps show the fluorescence increase evoked by a single ON shock on electrodes 1 (middle) and 2 (right). Each outlined glomerulus is activated by only one electrode.

(B) Response in glomerulus A (from [A]) is slightly reduced (right traces) when stimulated 400 msec after its neighbors (for example, glomerulus B) have been activated by stimulation on electrode 2 (left traces). This inhibition must be interglomerular because electrode 2 does not activate glomerulus A (the slight deflection in glomerulus A's fluorescence after electrode 2 stimulation [left] is scattered light from adjacent, activated glomeruli; note that no signal focus appears in the response map—see [A], right).

(C) SR of glomeruli tested in this series of experiments as a function of their distance to the nearest glomerulus activated by the conditioning stimulus. Lateral inhibition was significant only for those glomeruli within 400 μm of another glomerulus. Dashed line indicates no suppression. Error bars indicate SEM.

(D) Plot showing average SR versus ISI for those glomeruli showing an interglomerular SR < 0.9 at 400 msec ISI. Data for intraglomerular inhibition from Figure 3C are plotted on the dashed line for comparison.

(E) Blockade of ionotropic glutamate receptors (with NBQX/AP-5) or GABA_B receptors (with CGP55845) completely relieves lateral presynaptic inhibition in five experiments with strongly inhibited glomeruli.

course to the response to butyl acetate alone. To visualize any potential inhibition more globally, we summed the response maps evoked by each odorant and subtracted the map of the response to the mixture (Figure 5D). In this example, the difference map reveals little or no suppression in any glomeruli in the imaged region.

Because odorants evoke input to widespread glomeruli, we also searched for suppressive interactions when

imaging across the entire dorsal bulb (Figures 6A–6C). As in the previous example, directly adjacent glomeruli selectively activated by butyl acetate and methyl valerate show identical responses to the single odorant and to the binary mixture (Figure 6D). In addition, the global difference map (Figure 6E) shows that none of the selectively activated glomeruli show any suppression by the mixture. Two glomeruli that do show mixture

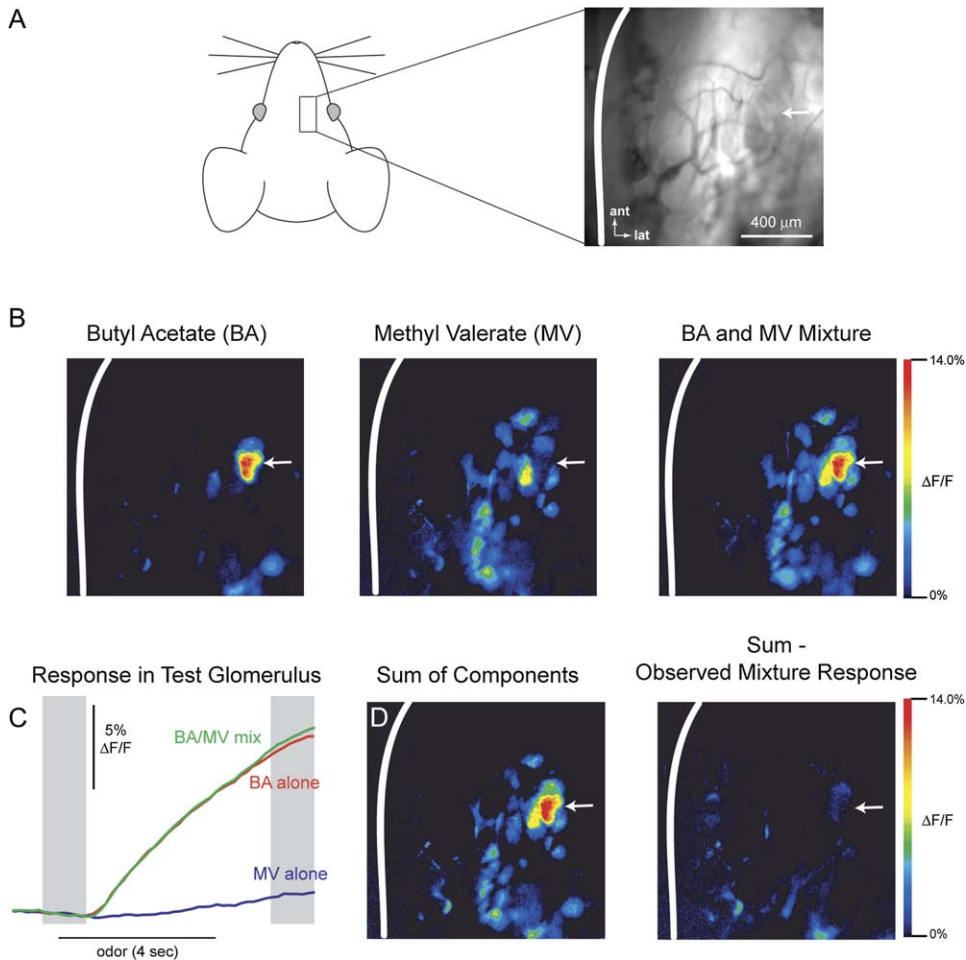


Figure 5. Odorant-Evoked Activation of Neighboring Glomeruli Does Not Inhibit Transmitter Release In Vivo

(A) Schematic and field of view of in vivo imaging experiment from the dorsal surface of the mouse olfactory bulb. Resting fluorescence of imaged area (field of view, 1340 μm) shown on right.

(B) Pseudocolor maps of the increase in fluorescence evoked by butyl acetate (BA, left, 0.7% s.v.), methyl valerate (MV, middle, 12% s.v.), or a mixture of BA and MV at the same concentrations (right). BA evoked strong signals in one glomerulus (white arrow) that was not activated by MV, and MV evoked signals in many surrounding glomeruli but not in the glomerulus responding to BA.

(C–D) Traces showing response of the glomerulus from (B) evoked by BA (red), MV (blue), or a mixture of BA and MV (green). Time of odorant presentation is indicated by the horizontal line, and shaded regions indicate the frames used to compute the response maps shown in (B) and (D). The response of this glomerulus to the mixture is no different than the response to BA alone. (D) Pseudocolor maps showing the pixel-by-pixel sum of responses to BA and MV (left) and the difference between this sum and the actual response to the mixture (right). The right map is the difference between the left map of (D) and the right map of (B). Suppressed glomeruli would appear bright in this difference map (D, right).

suppression are activated by both odorants (Figure 6E, arrows), an effect we observed in several preparations (see below).

To test for lateral inhibition between as many different glomeruli as possible, we performed the above experiment for six different odorant pairings (see Experimental Procedures) in five preparations. Our analysis included 79 glomeruli that responded selectively to one odorant in a pair. For each glomerulus, we calculated SR as the ratio of the response evoked by the binary mixture to that evoked by the test odorant alone. There was no significant suppression across these glomeruli (Figure 6F; $\text{SR} = 0.98 \pm 0.02$; $n = 79$; one-group t test; $p = 0.36$). Restricting the analysis to include only glomeruli within 400 μm of a glomerulus activated by the other odorant in the pair gave the same result (Figure 6F; $\text{SR} = 1.01 \pm 0.03$; $n = 44$; one group t test; $p = 0.70$). Our analysis

also included 19 glomeruli that were activated by both test odorants. For these glomeruli, we calculated SR as the ratio of the mixture response to that of the sum of the responses to each individual odorant and did find significant suppression (Figure 6G; mean $\text{SR} = 0.76 \pm 0.04$; one group t test; $p < 0.001$). This suppression likely reflects nonlinearities (i.e., saturation) in the concentration-response functions of the activated OSNs (Tabor et al., 2004) and may also reflect feedback, intraglomerular presynaptic inhibition of transmitter release, whose effects in vivo we describe below.

These results constitute a strong test of the hypothesis that presynaptic inhibition between neighboring glomeruli affects the input to the bulb and suggest that it does not. Instead, the magnitude of sensory input to a glomerulus appears to be independent of the input to neighboring glomeruli.

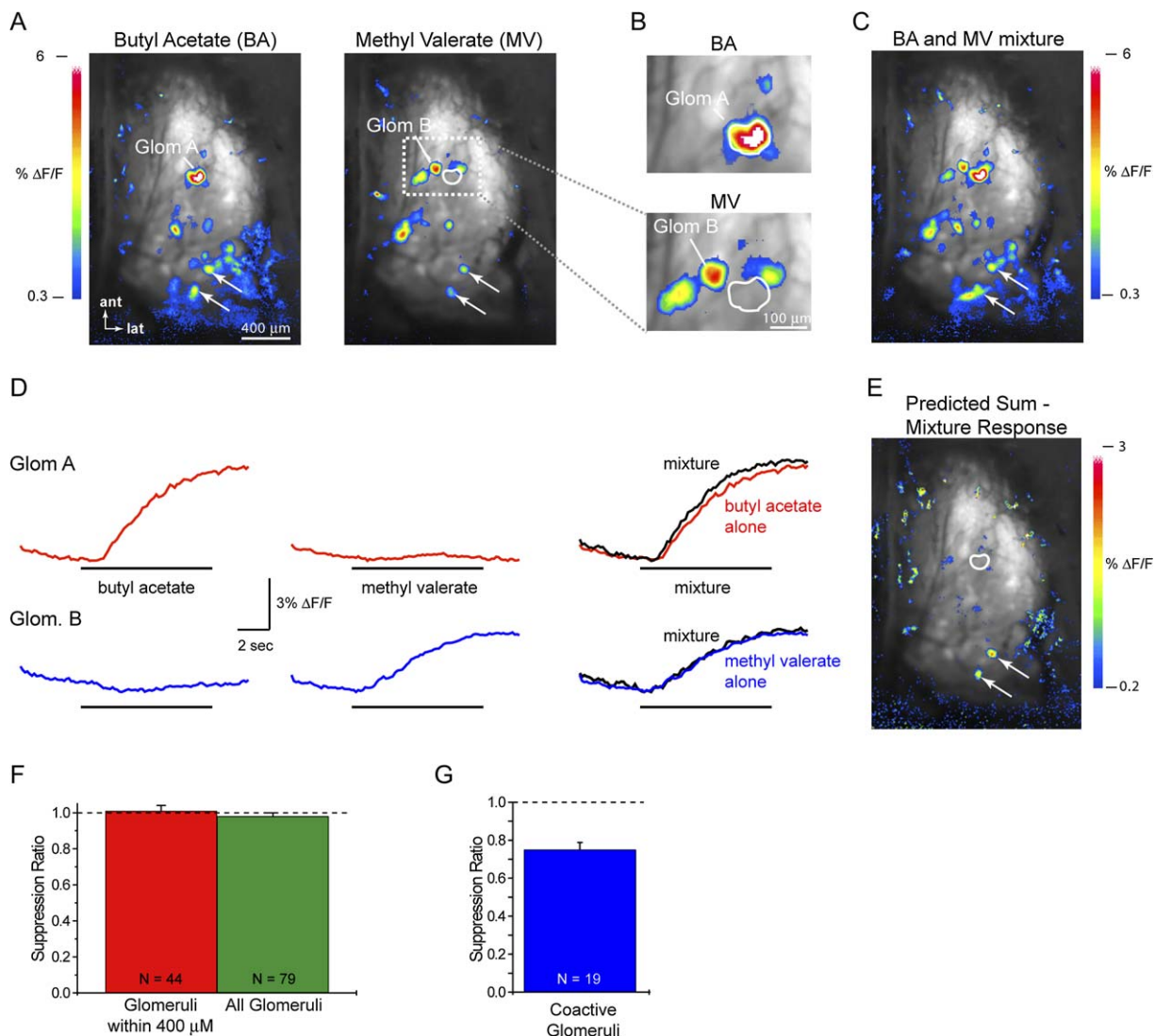


Figure 6. No Evidence for Interglomerular Presynaptic Inhibition on Any Spatial Scale

(A) Pseudocolor map of the spH signal evoked by butyl acetate (BA; 1% vapor dilution from BA diluted 1:100 in mineral oil) or methyl valerate (MV; 4% vapor dilution from MV diluted 1:200 in mineral oil), overlaid on an image of the resting fluorescence of the entire dorsal surface of one olfactory bulb (different preparation than in Figure 5; field of view, 1.7 × 2.4 mm). Arrows indicate two glomeruli activated by both odorants. Dashed box indicates region shown in (B). Each map is normalized to its own maximum.

(B) Enlarged image showing adjacent glomeruli selectively activated by BA (top) and MV (bottom).

(C) Pseudocolor map of the spH signal evoked by simultaneous presentation of BA and MV.

(D) Traces showing the spH signal evoked in glomeruli A (top) and B (bottom) by each odorant. Each glomerulus is selectively activated by one of the two odorants. For each glomerulus, the response to the binary mixture is no different from its response to the single component presented alone.

(E) Pseudocolor map showing the difference between the response to the mixture and the sum of the responses to BA and MV individually. The two glomeruli activated by both odorants (arrows) appear in this map, reflecting a sublinear addition of their response to each odorant. Scaling on this map is to half the level of the map in (C) to highlight even small levels of suppression. None of the glomeruli selectively activated by one odorant show suppression.

(F) Summary data showing SR calculated for all glomeruli activated by only one of the pair of odorants (green) and for the subset of these glomeruli within 400 μm of a glomerulus activated by the other odorant (red). Neither group shows any significant suppression.

(G) Summary data showing that glomeruli activated by both odorants in a pair show sublinear summation in their responses to the binary mixture.

Intraglomerular Presynaptic Inhibition Strongly Modulates Odorant-Evoked Input to Glomeruli

We next asked whether feedback inhibition within a glomerulus modulates odorant-evoked input. Because GABA_B antagonists eliminated heterosynaptic inhibition in slices, we addressed this question by comparing odorant-evoked spH signals before and after blocking GABA_B receptors in vivo. Drugs were applied directly to

the dorsal surface of the olfactory bulb. The GABA_B agonist baclofen, which strongly suppresses ON shock-evoked spH signals in vitro (Wachowiak et al., 2005), nearly eliminated odorant-evoked signals when applied at high concentration (1 mM), reducing spH signal amplitudes to 9.4% ± 5.5% of predrug levels (n = 9 glomeruli, one preparation). To confirm GABA_B receptor blockade in vivo, in one preparation (Figure 7A), we applied a lower

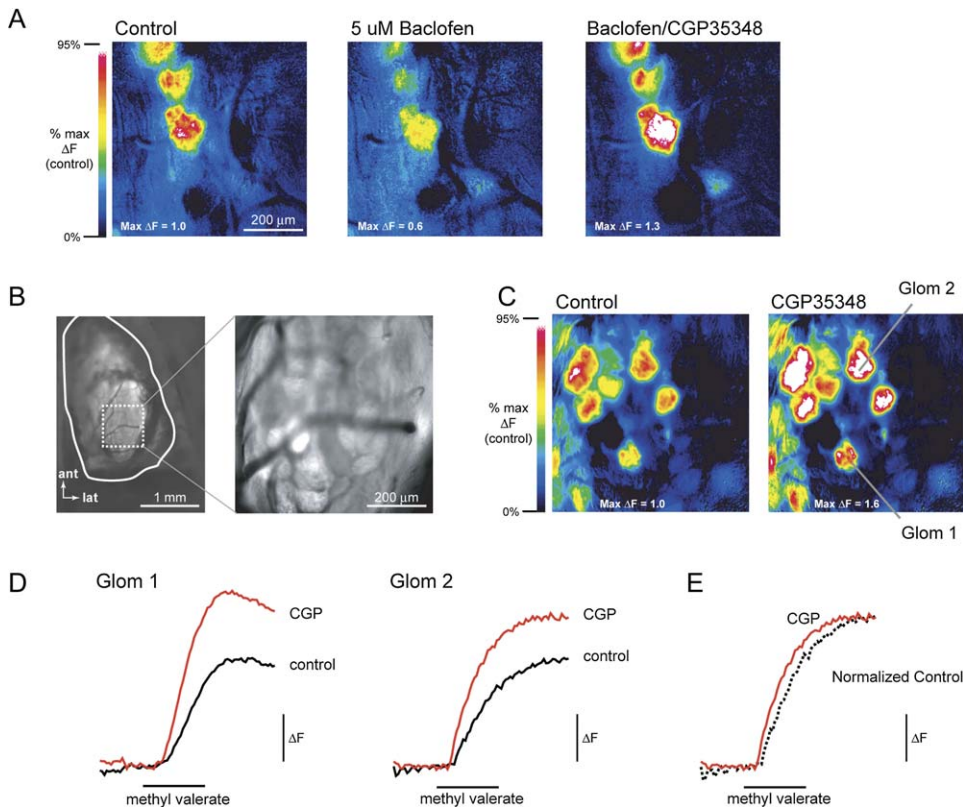


Figure 7. GABA_B Receptor Blockade Increases Odorant-Evoked Transmitter Release In Vivo

(A) Maps of the spH signal evoked by butyl acetate (0.4% s.v.). The GABA_B receptor agonist baclofen (5 μM) reduced the amplitude of the odorant-evoked response (middle) in all three activated glomeruli compared to control levels (left). The reduction was reversed by coapplication with the GABA_B receptor antagonist CGP35348 (1 mM; right). All maps scaled to the maximum of the control response. Normalized maximal signal amplitudes are shown at the bottom of each map. Maps and traces in this figure show ΔF (arbitrary units) to control for drug-induced changes in resting fluorescence (see text).

(B–D) Resting fluorescence of the dorsal olfactory bulb used in the experiment shown in (C) and (D). Inset shows resting fluorescence of the region imaged for data collection (field of view, 666 μm). (C) Maps of the spH signal evoked by methyl valerate (0.6% s.v.) before (left) and after (right) application of CGP35348. Maps are scaled to the maximum of the control response. Although CGP increased the amplitude of the odorant-evoked responses, the set of responsive glomeruli did not change. (D) Traces showing the effect of CGP35348 on the odorant-evoked spH signal in two glomeruli from (C). Horizontal bars indicate time of odorant presentation (4 s).

(E) Same traces from Glom 2 in (D) normalized to their maxima to illustrate the slight increase in the response kinetics produced by CGP35348.

baclofen concentration (5 μM), which reduced odorant-evoked signals to $58.0\% \pm 4.1\%$ of control values ($n = 3$ glomeruli), and then coapplied the water-soluble GABA_B antagonist CGP35348 (1 mM). CGP35348 reversed the effect of baclofen (response amplitude, $112.6\% \pm 12.7\%$ of control; $n = 3$ glomeruli), confirming that this concentration effectively blocked presynaptic GABA_B receptors when applied to the dorsal bulb.

In six additional experiments, we imaged odorant-evoked spH signals before and after application of CGP35348. CGP35348 dramatically increased the amplitude of the odorant-evoked signal (Figures 7B–7D). On average, CGP35348 increased the response amplitude to $178\% \pm 6.7\%$ of control ($n = 91$ glomeruli). The rise time of the response also decreased slightly, with the time to half maximum for a 4 s odorant presentation decreasing from 2.91 ± 0.08 s to 2.60 ± 0.07 s ($n = 65$ glomeruli in six preparations; paired *t* test, $p < 0.001$) (Figure 7E). Because GABA_B receptor blockade does not affect the recovery rate of the ON-evoked spH signal *in vitro* (see above), this result indicates an enhancement of OSN input to glomeruli after blocking GABAergic

presynaptic inhibition. Thus, intraglomerular inhibition regulates the magnitude of sensory input to the olfactory bulb.

GABA_B receptor blockade had little effect on relative spatial patterns (i.e., maps) of glomerular input (Figures 7C and 8A). We addressed this issue quantitatively by correlating response maps before and after CGP35348. Response amplitudes in every glomerulus exhibiting a response at any concentration were measured on every trial, yielding an array of response amplitudes for each trial. Response maps evoked by the same odorant and concentration before and after drug application were highly correlated (Figure 8C) (mean Pearson's $r = 0.82 \pm 0.01$; $n = 333$ comparisons; six preparations) and were nearly as similar as maps of repeated presentations before application (mean Pearson's $r = 0.88 \pm 0.01$; $n = 123$ comparisons; six preparations). The correlation between response maps from control and CGP35348 trials at the highest concentrations tested (3%–5.4% s.v.) was no different than the overall mean (paired *t* test; $p = 0.55$; four preparations). For comparison, response maps evoked by different odorants or

different concentrations showed much lower correlations (see [Figures 8A and 8B](#)).

Thus, although presynaptic inhibition mediated by GABA_B receptors strongly modulates the magnitude of odorant-evoked input to glomeruli, it does not significantly alter spatial maps of activity across glomeruli. This result is consistent with the slice experiments indicating that interglomerular, lateral presynaptic inhibition does not play a significant role modulating odorant-evoked input to the bulb.

Discussion

We have characterized how olfactory receptor neuron input to the CNS is regulated presynaptically by imaging transmitter release directly from OSN axon terminals. Both slice and *in vivo* experiments lead to similar conclusions. We find that input to the olfactory bulb is strongly modulated by feedback inhibition from bulbar interneurons; this inhibition is organized on a glomerular level, such that release from OSN terminals is greatly affected by feedback originating within the innervated glomerulus. In contrast, presynaptic inhibitory connections between glomeruli are much weaker than intraglomerular connections and do not appear strong enough to significantly shape spatial patterns of odorant-evoked input *in vivo*.

Using spH Imaging to Evaluate Input to the Bulb

Our conclusions are based on optical signals generated by the pH-sensitive GFP derivative synaptopHluorin ([Miesenbock et al., 1998](#)), expressed selectively in OSNs ([Bozza et al., 2004](#)). The utility of spH as a reporter of stimulus-evoked input to the bulb is well established ([Ng et al., 2002](#); [Bozza et al., 2004](#); [Wachowiak et al., 2005](#)). Nonetheless, its use as a reporter of transmitter release, as opposed to vesicle recycling ([Gandhi and Stevens, 2003](#); [Li et al., 2005](#)), is unusual and deserves further consideration. One potential confound in measuring transmitter release in response to prolonged (4 s, in these experiments) odorant stimulation is that release signals may be offset by fluorescence decreases because of vesicle endocytosis ([Miesenbock et al., 1998](#); [Sankaranarayanan and Ryan, 2000](#)). However, our *in vivo* experiments compared spH signals in conditions in which recycling was unchanged. Thus, changes in odorant-evoked spH signal amplitude after GABA_B receptor blockade can safely be interpreted as reflecting a modulation of transmitter release from OSN inputs.

A second potential confound in interpreting spH signal amplitudes is the effect of extracellular pH changes in the synaptic cleft. We found that the initial kinetics of the spH signal were shaped by a rapid, transient acidification followed by a slower transient alkalization. The acidification is likely due to the synchronous release of protons into the cleft after vesicle fusion, whereas the alkalization is due to the cotransport of protons out of the cleft by glutamate transporters. Both the rapid acidification and slower alkalization have also been reported at afferent terminals in hippocampal slices ([Krishtal et al., 1987](#)), but to our knowledge, this result is the first report of such phenomena shaping spH signals. Most earlier spH imaging studies have been performed on cultured neurons ([Miesenbock et al., 1998](#); [Sankaranarayanan](#)

[and Ryan, 2000](#); [Gandhi and Stevens, 2003](#)); extracellular pH effects may be enhanced in intact neuropile, and particularly so in the glomerulus, which has a high density of OSN terminals surrounded by a glial compartment ([Kasowski et al., 1999](#)). Despite this potential confound, in a recent study relating ON-evoked spH signal amplitude to monosynaptic EPSCs in external tufted cells, we found that the two measures show a nearly identical supralinear dependence on $[Ca^{2+}]_{ext}$ ([Wachowiak et al., 2005](#)). We also found that measuring spH response amplitude at latencies at which pH effects no longer contribute to the signal, or after minimizing these effects by increased buffering capacity, yielded identical conclusions about presynaptic inhibition of transmitter release in slices. Thus, the evidence is strong that spH signal amplitude, at least as measured in our slice experiments, effectively reports relative levels of stimulus-evoked release.

SpH signals evoked in olfactory bulb slices were smaller than those observed *in vivo* (by a factor of 2–10). This discrepancy likely reflects differences between patterns of OSN activation evoked by electrical versus odorant stimulation. Nerve shocks evoke single volleys of synchronous action potentials in a small subset of afferents near the electrode, whereas odorant stimulation evokes prolonged activation of many, and potentially all, afferents innervating a glomerulus. In addition, the slow time-course of vesicle endocytosis permits “summation” of the spH signal during odorant stimulation ([Bozza et al., 2004](#)), enhancing signal amplitude relative to the shock-evoked response.

Multiple Pathways Modulating OSN Input to the Olfactory Bulb

Activity-dependent suppression of release from OSNs consists of both a synaptic feedback component and a paired-pulse depression intrinsic to the presynaptic terminal. Paired-pulse depression was evident immediately after a conditioning pulse and reached maximal strengths of ~50% reduction in release. In contrast, heterosynaptic feedback inhibition suppressed transmitter release by 60%–70%. Feedback inhibition was maximal 50–100 msec after a stimulus and strongly suppressed release for up to several seconds, consistent with its being mediated by presynaptic metabotropic receptors. GABA_B antagonists eliminated nearly all feedback inhibition, implicating GABAergic periglomerular cells as the primary interneuron type involved. We did not investigate whether D₂ dopamine receptors also mediate feedback inhibition, although earlier studies suggest that they can modulate OSN input ([Ennis et al., 2001](#); [Hsia et al., 1999](#); [Wachowiak and Cohen, 1999](#)), and some PG cells receiving direct OSN input are dopaminergic ([Toida et al., 2000](#)). The fact that feedback inhibition suppressed release from OSN axons other than those providing the initial input suggests that OSN input evokes inhibition that spreads throughout the glomerulus. This organization strengthens the notion of the glomerulus as a functional unit, in that even intraglomerular synaptic interactions appear to spread through the entire glomerular neuropile.

In slices, lateral inhibition between neighboring glomeruli could modulate transmitter release from OSNs but only weakly compared to the strength of intraglomerular

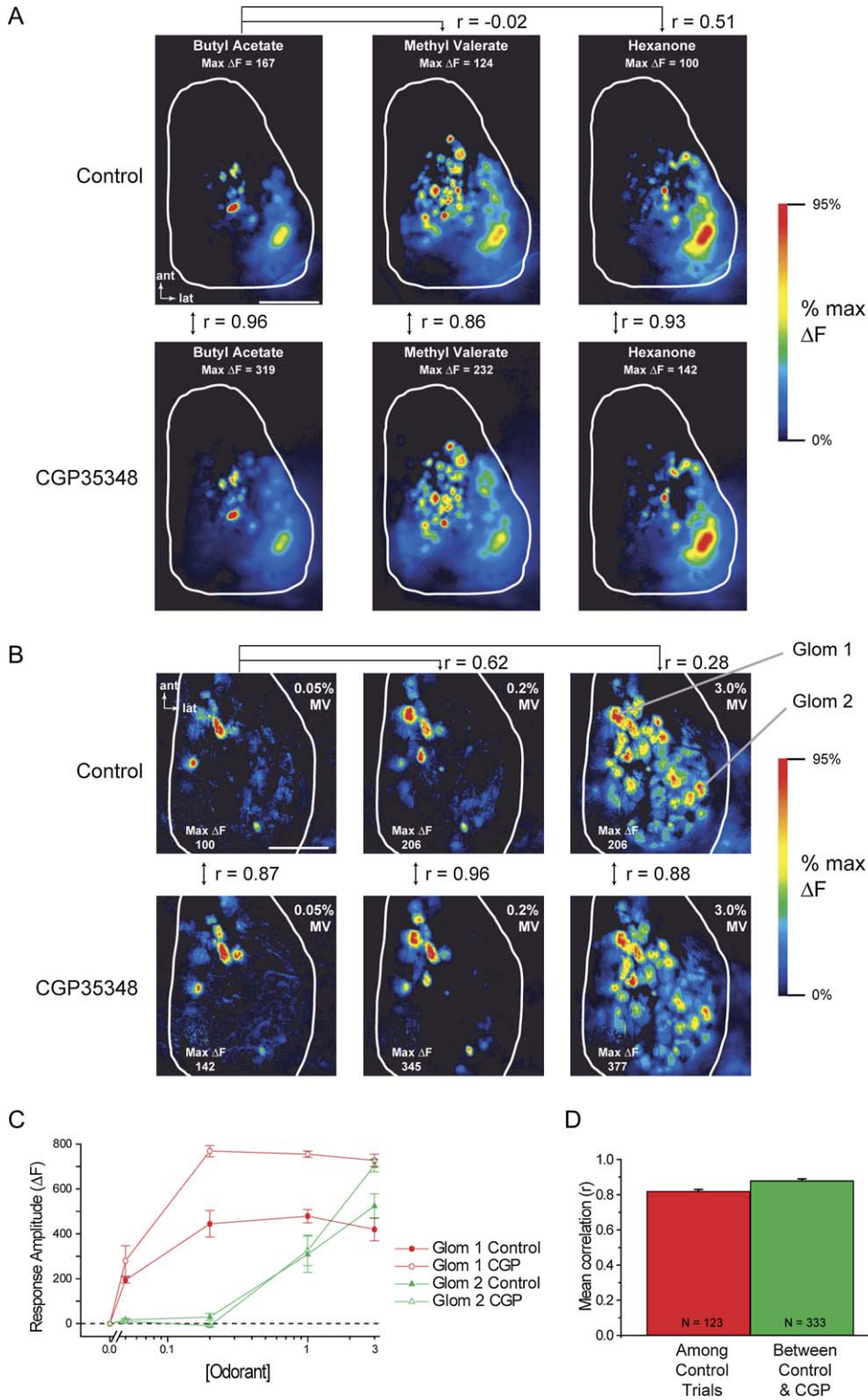


Figure 8. GABA_B Receptor Blockade Increases Odorant-Evoked Responses while Maintaining Relative Maps of Input to Glomeruli
(A) Maps of the spH signal evoked by different odorants in the same preparation before (upper panels) and after (lower panels) GABA_B receptor blockade by CGP35348. Absolute response amplitudes increased in CGP35348 (as shown by the increase in the maximum evoked fluorescence, ΔF , in each map), but each map is scaled to its own maximum to compare relative response amplitudes across glomeruli before and after CGP35348 application. The number between each vertical pair reports the correlation coefficient between the responses of 29 odorant-activated glomeruli before and after drug application. Numbers across the top report the corresponding correlations between different odorants under control conditions for comparison. All odorants were presented at 0.5% s.v. Scale bar, 1 mm. The approximate border of the dorsal bulb is indicated in white.

feedback inhibition or paired-pulse depression. In addition, although lateral presynaptic inhibition was weak *in vitro*, we could find no evidence that it modulated odorant-evoked OSN input to glomeruli *in vivo*. How could we observe lateral inhibition *in vitro* but not *in vivo*? The explanation may lie in the circuitry underlying intra- versus interglomerular inhibition. Interglomerular inhibitory interactions are mediated by the short-axon cells, which are glutamatergic, branch extensively in the glomerular layer, and excite PG cells in glomeruli several hundred μm distant (Aungst et al., 2003) but do not receive monosynaptic OSN input (Hayar et al., 2004a). Indirect excitatory input to a glomerulus via the short-axon cells is likely weaker than direct input via thousands of convergent OSNs, and the slower-onset, asynchronous OSN input evoked by odorant stimulation may fail to evoke sufficient activation of PG cells in neighboring glomeruli to elicit presynaptic inhibition. Interestingly, however, interglomerular connections can potently inhibit mitral cell responses in neighboring glomeruli (Aungst et al., 2003), suggesting that postsynaptic interglomerular inhibition may be more robust than presynaptic inhibition. One possible explanation for this difference is that PG cells directly contact mitral cell dendrites (Pinching and Powell, 1971), whereas PG cell-mediated presynaptic inhibition is likely mediated via a synaptic spillover mechanism (Aroniadou-Anderjaska et al., 2000; Wachowiak et al., 2005). These differences point to the complexity of the glomerular neuronal network; for example, PG cells are a heterogeneous population (Hayar et al., 2004a), and short-axon cells may activate PG cells that inhibit mitral cells but do not presynaptically inhibit OSNs. Thus, interglomerular inhibition may shape odorant representations at the level of output from the glomerulus even while input to the glomerulus is unaffected.

Presynaptic Inhibition and Odor Coding

How does presynaptic inhibition shape odor representations? Our data suggest that a primary role is to modulate the strength of olfactory input to the CNS without altering the relative spatial patterns of glomerular activity that are thought to encode odor identity. Blocking presynaptic inhibition pharmacologically greatly enhanced the magnitude of odorant-evoked transmitter release and only minimally affected maps of odorant-evoked input. One important implication of this result is that the mapping of odorant identity onto space in the olfactory bulb, at least at the level of glomerular input, is determined primarily by the convergence of OSNs onto glomeruli rather than by postsynaptic processing. Presynaptic inhibition serves to modulate the strength of this input.

The massive convergence of OSNs onto glomeruli (Shepherd et al., 2004) and the unusually high release probability of OSNs (Murphy et al., 2004) are specializa-

tions that likely improve odorant detection, but these specializations invite saturation of postsynaptic responses at odorant concentrations above threshold. Thus, feedback presynaptic inhibition may be important in maintaining postsynaptic responsiveness at supra-threshold concentrations. Feedback inhibition may also be important in shaping olfactory bulb activity during repeated odorant stimulation. Mice and other mammals repeatedly sample odorants by rapid sniffing at frequencies of 4–10 Hz (Youngentob et al., 1987; Uchida and Mainen, 2003), which corresponds to the interval of maximal feedback inhibition. Presynaptic inhibition may reduce postsynaptic responses during sustained rapid sniffing and enhance detection of new odorants via different glomeruli by reducing downstream lateral inhibition (Aroniadou-Anderjaska et al., 2000). Alternatively, by preventing saturation of postsynaptic responses, presynaptic inhibition could enhance the responsiveness of mitral and tufted cells, the principal output neurons of the olfactory bulb. A similar mechanism enables sustained postsynaptic responses of second-order neurons activated by primary auditory afferents (Brenowitz and Trussell, 2001). Finally, the delayed (~ 50 msec) onset of presynaptic inhibition could shape temporal patterns of input. In the hippocampus, for example, GABA_B-mediated presynaptic inhibition functions as a high-pass filter for transmission of afferent signals (Ohliger-Ferking et al., 2003). In the olfactory system such filtering could enhance the phasic component of OSN inputs and help entrain postsynaptic neurons to the ongoing sniff rhythm (Hayar et al., 2004b; Schoppa and Westbrook, 2001).

Presynaptic inhibition may also modulate the sensitivity to olfactory input on a slower time scale. For example, input sensitivity could be modulated by activity-dependent changes in the production of transmitters mediating presynaptic inhibition, as has been shown for dopaminergic periglomerular cells (Cho et al., 1996), or by changes in tonic levels of GABAergic inhibition (Aroniadou-Anderjaska et al., 2000). In this context, the predominance of intraglomerular over interglomerular presynaptic inhibition may enable glomerulus-specific control of olfactory input, potentially allowing for the selection of inputs arising from select olfactory receptor populations.

Experimental Procedures

Subjects

Experiments were performed on 71 transgenic mice expressing synaptotagmin (spH) from the OMP locus, as previously reported (Bozza et al., 2004). OMP-spH mice are available commercially (The Jackson Laboratory, Bar Harbor, Maine, stock #4946). For the slice experiments, mice used ranged from 3 to 17 weeks old (mean: 7 weeks). For the *in vivo* experiments, mice ranged from 8 to 19 weeks old (mean: 14 weeks). Although most mice were

(B) SpH signal maps evoked by methyl valerate (MV) at different concentrations before (upper panels) and during (lower panels) GABA_B receptor blockade by CGP35348. As in (A), each map is scaled to its own maximum and maximal response amplitude is indicated for each map. Numbers between and above maps indicate correlation coefficients for select map pairs as in (A). Scale bar, 400 μm .

(C) Concentration-response functions from two glomeruli (indicated in [B]) before and during CGP35348 application. Error bars indicate SEM and are computed from three to four repeated trials at each concentration.

(D) Summary data showing the mean correlation between glomerular response patterns (six preparations) evoked by the same odorant and concentration between control and drug trials and among repeated control trials for all possible trial-to-trial comparisons. N indicates the number of pairwise comparisons made.

homozygous for spH (and were thus OMP null), a subset of experiments performed in ten heterozygous mice produced similar results, consistent with our previous report (Bozza et al., 2004). To improve visibility of OSN axons in slice experiments, in some cases, we loaded mouse OSNs with the red fluorescent marker Alexa 568 dextran (10 kDa, Molecular Probes, Eugene, Oregon) 1–7 days prior to the experiment, as previously reported (Wachowiak and Cohen, 2001). All animal procedures were approved by the Boston University Institutional Animal Care and Use Committee.

Slice Preparation and Recording

Mice were anesthetized with halothane and decapitated. The head was immediately submerged in ice-cold aCSF (composition, in mM: 124 NaCl, 3 KCl, 2 CaCl₂, 1.3 MgSO₄, 10 dextrose, 26 NaHCO₃, 1.25 NaH₂PO₄) equilibrated with a mixture of 95% oxygen and 5% carbon dioxide. The olfactory bulbs were quickly removed and submerged in ice-cold aCSF. Each bulb was glued to a plastic block with cyanoacrylate and sectioned with a custom vertical rotary slicer. Three 400 μ m thick sections were obtained from each bulb in either a sagittal or horizontal orientation, including a “surface slice” cut tangentially to the surface of the bulb. Slices were stored in an incubation chamber in aCSF at 35°C for 30 min after slicing, after which the temperature was reduced to 30°C.

For imaging, slices were transferred to a recording chamber and continuously perfused with aCSF at approximately 2 ml/minute. Slices were maintained at 30°C throughout the recording (except in experiments that explicitly varied temperature, see Results). For experiments that used aCSF with extra pH-buffering capacity, 20 mM HEPES was added to the aCSF, replacing 5 mM dextrose and 7.5 mM NaCl to maintain osmolarity, and the oxygenated solution was pH-matched to the control aCSF.

Electrical stimuli were applied through concentric bipolar electrodes with a tip diameter of 25 μ m (Frederick Haer, Bowdoinham, Maine). Brief (100 μ sec) constant current stimuli (5–400 μ A) were delivered through Isoflex stimulus isolation units (A.M.P.I., Jerusalem, Israel) under the control of custom software written in LabView (National Instruments, Austin, Texas).

Slices were imaged by wide-field epillumination fluorescence with an Olympus BX51 microscope and a 10 \times (0.3 NA) or 20 \times (0.95 NA) objective. Illumination was provided by a 150W Xenon arc lamp (Opti-Quip, New York) attenuated by 98.5%–75% with neutral density filters. SpH was visualized with a filter set containing HQ480/40 (excitation), Q505LP (dichroic), and HQ535/50 (emission) filters. Optical signals were recorded with a back-illuminated CCD camera (NeuroCCD, SM-80, RedShirtImaging, Fairfield, Connecticut), at 80 \times 80 pixel resolution and digitized by 14 bit analog-to-digital conversion at a frame rate of 125 or 500 Hz. Data acquisition was performed with Neuroplex software (RedShirtImaging).

Optical Imaging In Vivo

In vivo imaging from the dorsal olfactory bulb was performed in pentobarbital-anesthetized mice, as described previously (Bozza et al., 2004; Wachowiak and Cohen, 2001). For the mixture experiments, signals were recorded through thinned bone. For the in vivo pharmacology experiments, the bone and dura were removed prior to imaging. In most (8 of 10) mice, a double tracheotomy was performed and a 3 Hz artificial sniffing protocol was used to control odorant inhalation (Wachowiak and Cohen, 2001). In the other two experiments, mice were freely breathing at \sim 2 Hz. Optical signals were recorded with a back-illuminated CCD camera (NeuroCCD, SM-256, RedShirtImaging, Fairfield, Connecticut) at 256 \times 256 pixel resolution and a frame rate of 7 Hz. Data were acquired and digitized as described above.

The binary mixture experiments used the following odorant pairs (n given in parentheses): methyl valerate/butyl acetate (2), methyl valerate/isoamyl acetate (1), methyl benzoate/ α -pinene (1), methyl benzoate/2-heptanone (1), methyl valerate/2-heptanone (1), and methyl valerate paired with a mixture of five of the preceding odorants (1). All odorants were obtained at 95%–99% purity from Sigma (St. Louis, Missouri) and stored under nitrogen. For delivery, a nitrogen stream was passed through a vial containing each odorant and was then diluted to the working concentration in cleaned, desiccated air with a mass flow controller (Aalborg, Orangeburg, NY) under computer control as described previously (Bozza et al., 2004).

Concentrations are expressed as percent dilutions of concentrated vapor.

Drug Application

All drugs were obtained from Tocris Cookson (Ellisville, Missouri) or Sigma (St. Louis, Missouri). In slice experiments, drugs were diluted from frozen stocks and bath applied. During in vivo imaging, drugs were applied by manually replacing our standard mouse ringers superfusate (Bozza et al., 2004) with ringers containing CGP35348 or baclofen.

Data Analysis

In most cases, the signal-to-noise ratio of the data was improved by averaging two to eight trials. Raw traces were corrected for photobleaching by subtracting trials in which no stimulus was given. Fluorescence traces from each pixel overlying a glomerulus were averaged. Data from slice experiments were temporally low-pass filtered at 20 Hz using a Gaussian filter with a low sharpness. Response amplitudes in slice experiments were measured as the peak deflection from baseline averaged over a 40 msec window after the stimulus. Suppression of transmitter release in slice experiments was quantified in terms of the suppression ratio, defined as the amplitude of the response to a test stimulus divided by the response to a control stimulus. In most cases, trials with and without the conditioning stimulus were interleaved and then averaged separately. Trials were separated by a minimum of 60 s. No spatial filtering was performed, although for display purposes the pixel resolution of response maps was doubled via linear interpolation.

In the in vivo experiments, odorant response amplitudes were measured using a 1.4 s temporal window positioned just after the end of odorant presentation. spH response maps were constructed by subtracting the temporal average of a 2 s time window just preceding stimulus onset from a 2 s time window at the peak of the response. As in the slice experiments, no spatial filtering was performed, although the pixel resolution of response maps was doubled for display.

To analyze effects of CGP35348 in vivo, odorant-evoked spH signals were measured for each single trial for each responsive glomerulus. Glomeruli were included in the final analysis if their response amplitude was greater than three standard errors above zero given at least three repeated odorant presentations. Correlation coefficients (Pearson's *r*) were computed from the set of all responsive glomeruli in a given preparation.

In all cases except for the in vivo pharmacology experiments (see Figures 7 and 8), data were divided by the resting fluorescence for display in the figures, in order to convey a useful sense of the signal size. However, this number has limited interpretive meaning because evoked spH signals arise from a pool of intravesicular protein that is largely nonfluorescent (Sankaranarayanan and Ryan, 2000). Resting fluorescence did not change appreciably with stimulation or drug treatment in the slice preparations (not shown). Because resting fluorescence could vary after drug treatment in the in vivo experiments (not shown), data were analyzed and presented without dividing by resting fluorescence.

Data processing and analysis were performed with Neuroplex software and custom software written in LabVIEW and MatLab (The Mathworks, Natick, Massachusetts). Statistical comparisons were performed with Origin and StatView. Least-squares curve fits were performed with Igor Pro.

Acknowledgments

We thank Michael Shipley, Larry Cohen, Todd Blute, and Jen-Wei Lin for helpful discussion. This work was funded by National Institute on Deafness and Other Communication Disorders grants DC6441 and DC4938 to M.W. and National Research Service Award DC7258 to J.P.M.

Received: June 23, 2005

Revised: September 19, 2005

Accepted: October 19, 2005

Published: December 21, 2005

References

- Aroniadou-Anderjaska, V., Zhou, F.M., Priest, C.A., Ennis, M., and Shipley, M.T. (2000). Tonic and synaptically evoked presynaptic inhibition of sensory input to the rat olfactory bulb via GABA(B) heteroreceptors. *J. Neurophysiol.* *84*, 1194–1203.
- Aungst, J.L., Heyward, P.M., Puche, A.C., Karnup, S.V., Hayar, A., Szabo, G., and Shipley, M.T. (2003). Centre-surround inhibition among olfactory bulb glomeruli. *Nature* *426*, 623–629.
- Bozza, T., Feinstein, P., Zheng, C., and Mombaerts, P. (2002). Odorant receptor expression defines functional units in the mouse olfactory system. *J. Neurosci.* *22*, 3033–3043.
- Bozza, T., McGann, J.P., Mombaerts, P., and Wachowiak, M. (2004). In vivo imaging of neuronal activity by targeted expression of a genetically encoded probe in the mouse. *Neuron* *42*, 9–21.
- Brenowitz, S., and Trussell, L.O. (2001). Minimizing synaptic depression by control of release probability. *J. Neurosci.* *21*, 1857–1867.
- Chen, W.R., Xiong, W., and Shepherd, G.M. (2000). Analysis of relations between NMDA receptors and GABA release at olfactory bulb reciprocal synapses. *Neuron* *25*, 625–633.
- Cho, J.Y., Min, N., Franzen, L., and Baker, H. (1996). Rapid down-regulation of tyrosine hydroxylase expression in the olfactory bulb of naris-occluded adult rats. *J. Comp. Neurol.* *369*, 264–276.
- Duchamp-Viret, P., Delaleu, J.-C., and Duchamp, A. (2000). GABA_B-mediated action in the frog olfactory bulb makes odor responses more salient. *Neuroscience* *97*, 771–777.
- Ennis, M., Zhou, F.M., Ciombor, K.J., Aroniadou-Anderjaska, V., Hayar, A., Borrelli, E., Zimmer, L.A., Margolis, F., and Shipley, M.T. (2001). Dopamine D2 receptor-mediated presynaptic inhibition of olfactory nerve terminals. *J. Neurophysiol.* *86*, 2986–2997.
- Gandhi, S.P., and Stevens, C.F. (2003). Three modes of synaptic vesicular recycling revealed by single-vesicle imaging. *Nature* *423*, 607–613.
- Getchell, T.V., and Shepherd, G.M. (1975). Short-axon cells in the olfactory bulb: dendrodendritic synaptic interactions. *J. Physiol.* *251*, 523–548.
- Hayar, A., Karnup, S., Ennis, M., and Shipley, M.T. (2004a). External tufted cells: a major excitatory element that coordinates glomerular activity. *J. Neurosci.* *24*, 6676–6685.
- Hayar, A., Karnup, S., Shipley, M.T., and Ennis, M. (2004b). Olfactory bulb glomeruli: external tufted cells intrinsically burst at theta frequency and are entrained by patterned olfactory input. *J. Neurosci.* *24*, 1190–1199.
- Hsia, A.Y., Vincent, J.D., and Lledo, P.M. (1999). Dopamine depresses synaptic inputs into the olfactory bulb. *J. Neurophysiol.* *82*, 1082–1085.
- Isaacson, J.S., and Strowbridge, B.W. (1998). Olfactory reciprocal synapses: dendritic signaling in the CNS. *Neuron* *20*, 749–761.
- Kasowski, H.J., Kim, H., and Greer, C.A. (1999). Compartmental organization of the olfactory bulb glomerulus. *J. Comp. Neurol.* *407*, 261–274.
- Keller, A., Yagodin, S., Aroniadou-Anderjaska, V., Zimmer, L.A., Ennis, M., Sheppard, N.F., Jr., and Shipley, M.T. (1998). Functional organization of rat olfactory bulb glomeruli revealed by optical imaging. *J. Neurosci.* *18*, 2602–2612.
- Krishtal, O.A., Osipchuk, U.V., Shelest, T.N., and Smirnov, S.V. (1987). Rapid extracellular pH transients related to synaptic transmission in rat hippocampal slices. *Brain Res.* *436*, 352–356.
- Li, Z., Burrone, J., Tyler, W.J., Hartman, K.N., Albeanu, D.F., and Murthy, V.N. (2005). Synaptic vesicle recycling studied in transgenic mice expressing synaptopHluorin. *Proc. Natl. Acad. Sci. USA* *102*, 6131–6136.
- Miesenbock, G., De Angelis, D.A., and Rothman, J.E. (1998). Visualizing secretion and synaptic transmission with pH-sensitive green fluorescent proteins. *Nature* *394*, 192–195.
- Mombaerts, P., Wang, F., Dulac, C., Chao, S.K., Nemes, A., Mendelsohn, M., Edmonson, J., and Axel, R. (1996). Visualizing an olfactory sensory map. *Cell* *87*, 675–686.
- Murphy, G.J., Glickfield, L.L., Balsen, Z., and Isaacson, J.S. (2004). Sensory neuron signaling to the brain: properties of transmitter release from olfactory nerve terminals. *J. Neurosci.* *24*, 3023–3030.
- Murphy, G.J., Darcy, D.P., and Isaacson, J.S. (2005). Intraglomerular inhibition: signaling mechanisms of an olfactory microcircuit. *Nat. Neurosci.* *8*, 354–364.
- Ng, M., Roorda, R.D., Lima, S.Q., Zemelman, B.V., Morcillo, P., and Miesenbock, G. (2002). Transmission of olfactory information between three populations of neurons in the antennal lobe of the fly. *Neuron* *36*, 463–474.
- Ohliger-Frerking, P., Wiebe, S.P., Staubli, U., and Frerking, M. (2003). GABA(B) receptor-mediated presynaptic inhibition has history-dependent effects on synaptic transmission during physiologically relevant spike trains. *J. Neurosci.* *23*, 4809–4814.
- Pinching, A.J., and Powell, T.P.S. (1971). The neuropil of the periglomerular region of the olfactory bulb. *J. Cell Sci.* *9*, 379–409.
- Sankaranarayanan, S., and Ryan, T.A. (2000). Real-time measurements of vesicle-SNARE recycling in synapses of the central nervous system. *Nat. Cell Biol.* *2*, 197–204.
- Shepherd, G.M., Chen, W.R., and Greer, C.A. (2004). Olfactory bulb. In *The Synaptic Organization of the Brain*, G.M. Shepherd, ed. (New York: Oxford University Press), pp. 165–216.
- Schoppa, N.E., and Westbrook, G.L. (2001). Glomerulus-specific synchronization of mitral cells in the olfactory bulb. *Neuron* *31*, 639–651.
- Tabor, R., Yaksi, E., Weislogel, J.M., and Friedrich, R.W. (2004). Processing of odor mixtures in the zebrafish olfactory bulb. *J. Neurosci.* *24*, 6611–6620.
- Toida, K., Kosaka, K., Aika, Y., and Kosaka, T. (2000). Chemically defined neuron groups and their subpopulations in the glomerular layer of the rat main olfactory bulb—IV. Intraglomerular synapses of tyrosine hydroxylase-immunoreactive neurons. *Neuroscience* *101*, 11–17.
- Treloar, H.B., Feinstein, P., Mombaerts, P., and Greer, C.A. (2002). Specificity of glomerular targeting by olfactory sensory axons. *J. Neurosci.* *22*, 2469–2477.
- Uchida, N., and Mainen, Z.F. (2003). Speed and accuracy of olfactory discrimination in the rat. *Nat. Neurosci.* *6*, 1224–1229.
- Vucinić, D., Cohen, L.B., and Kosmidis, E.F. (2005). Interglomerular center-surround inhibition shapes odorant-evoked input to the mouse olfactory bulb in vivo. *J. Neurophysiol.*, in press. Published online November 30, 2005. 10.1152/jn.00918.2005.
- Wachowiak, M., and Cohen, L.B. (1999). Presynaptic inhibition of primary olfactory afferents mediated by different mechanisms in lobster and turtle. *J. Neurosci.* *19*, 8808–8817.
- Wachowiak, M., and Cohen, L.B. (2001). Representation of odorants by receptor neuron input to the mouse olfactory bulb. *Neuron* *32*, 723–735.
- Wachowiak, M., Denk, W., and Friedrich, R.W. (2004). Functional organization of sensory input to the olfactory bulb glomerulus analyzed by two-photon calcium imaging. *Proc. Natl. Acad. Sci. USA* *101*, 9097–9102.
- Wachowiak, M., McGann, J.P., Heyward, P.M., Shao, Z., Puche, A., and Shipley, M.T. (2005). Inhibition of olfactory receptor neuron input to olfactory bulb glomeruli mediated by suppression of presynaptic calcium influx. *J. Neurophysiol.* *94*, 2700–2712.
- Youngentob, S.L., Mozell, M.M., Sheehe, P.R., and Hornung, D.E. (1987). A quantitative analysis of sniffing strategies in rats performing odor detection tasks. *Physiol. Behav.* *41*, 59–69.
- Zerangue, N., and Kavanaugh, M.P. (1996). Flux coupling in a neuronal glutamate transporter. *Nature* *383*, 634–637.

Note Added in Proof

While this paper was in press, Vucinić et al. (2005) reported that in vivo pharmacological blockade of GABA_B-mediated presynaptic inhibition produced modest changes in maps of OSN input to glomeruli measured by imaging presynaptic calcium influx in neonatal mice. These changes were interpreted as evidence of interglomerular presynaptic inhibition. We replicated their analyses with the in vivo spH data presented in this study and found no such changes in maps at the level of transmitter release from OSNs.